Structural Analysis of Formula 1 Halo Protection Device

Nitin Ambhore*, *Nitin* Bhorse, *Nandika* Joshi, *Aman* Naranje, *Paritosh* Musmade, *Armaan* Mujawar, *Jahnvi* Nadkarni

Department of Mechanical Engineering, Vishwakarma Institute of Technology, Pune 411037, MS, India

Abstract. The Formula 1 Halo is a lifesaving technology in the engineering of motorsport vehicles, as it offers protection to the driver without compromising the motorsport performance. This is a structural, aerodynamic and vibrational examination of the F1 Halo that incorporates the multidisciplinary design validation. The Halo is verified to meet the requirements of FIA safety with maximum stress of 399.14 MPa (yield strength: 1030 MPa) and deformation of 2.687 mm (limit: 3.0 mm) under 125 kN vertical and 0 separation forces. Calculation fluid dynamics demonstrates 0.368-0.841 coefficients of aerodynamic drag at 30 m /s and 80 m /s and forces are about 1-2 percent of total drag on the vehicle. The modal analysis determines six natural frequencies that are between 63.81 Hz and 373.9 Hz, which proves that they effectively separate resonance frequencies that are associated with natural frequencies and those involved in operation. Grade 5 Titanium (Ti-6Al-4V) showed a high-end performance feature, which proved the structural performance and aerodynamic viability. This combined method shows that the strict computational design can prove the multi-objective design optimization of safety-critical.

1 Introduction

Formula 1 racing is at the very edge of automotive engineering and cars regularly hit high speeds of over 300 km/h when used in open cockpit versions. Three fatal and numerous serious head injuries caused by airborne debris in the period between 2007 and 2017 are indicators of the extreme vulnerability of this type of racing [1]. The Federation Internationale de l'Automobile (FIA) responded by ensuring that the Halo protection device was introduced in 2018 [2]. The Halo is a three-dimensional titanium framework attached to the vehicle chassis, which frames around the cockpit of the driver and prevents objects of large size and at the same time, absorbs the impact energy without affecting the visibility of the driver and the performance of the vehicle. Such a device is a great engineering accomplishment and there must be multifaceted optimization in several domains of design: structural strength, crash protection, aerodynamic efficiency, dynamic stability and manufacturing feasibility. Although the protective properties of the Halo have been proven by considerable physical crash tests, a comprehensive analysis of its integrated performance

* Corresponding author: nitin.ambhore@vit.edu

properties is still a rare publication [3-4]. This work will fill this gap by applying systematic finite element analysis (FEA) and computational fluid dynamics (CFD) investigations in conjunction with modal analysis to evaluate vibrational behavior. The combination strategy would prove the Halo within the regulations of the FIA on a quantitative level and be able to create baseline information regarding the needed optimization of future design. Literature Review

The creation of the Halo was based on the extensive examination of the motorsport fatalities. From 2007 to 2017, the cause of airborne debris was found to cause serious head injuries in roughly 35 percent of Formula 1 racing accidents [5]. Other past protective concepts, such as the shield design, never met the requirements of the driver visibility and structural performance. The curved form of the Halo offers protection on top as well as in front of it, similar to a wing, but also ensures visibility of the cockpit, which is vital in relation to competitive racing.

Grade 5 Titanium (Ti-6Al-4V) is the best solution that ought to be used to make Halo applications [6]. This alloy offers a strength-to-weight ratio with Young's modulus of 110 GPa and densities of 4430 kg/m3, yield strength of 1030 MPa to give high load carrying capacity, and a crystallographic structure that gives great impact resistance and energy absorption. The content has a good balance of performance and production cost as well, in order to be manufactured. Titanium offers superior material in terms of safety-critical loads as compared to other materials (aluminum 7075-T73, composite structures) as shown through systematic comparison [7-9]. SST k-o model of turbulence has emerged as the industry standard in the layout of external automotive aerodynamics with a proven better accuracy over the alternative models (k-e, Spalart-Allmaras) of separated flow in prediction. Authored literature confirms the development of an optimal mesh resolution (with inflation layers) with y + less than 1, which is found to make results that are consistent with wind tunnel values by a variance of 2-5% with respect to comparison of drag coefficients. Design validation using finite element analysis [10-11]. According to best practices (mesh sensitivity studies, convergence verifying studies, consistency with theoretical analysis), design validation studies with finite element analysis have the same confidence as physical testing, and are valuable in parametric studies because they are both less expensive and consume less time.

2 Methodology

2.1 Geometric modeling and domain definition

The Halo geometry was created in SolidWorks in accordance with the FIA standards of size and physical characteristics. The main support pillar has a curved shape whose profile is about 650 mm high above the chassis. The chassis mounting points are attached by two lateral side arms, and the tube geometry has a nominal outer diameter of 90 mm and an inner diameter of 82 mm with 4 mm wall thickness. The total weight of the halo is 7 kg, and it is made in such a way as to maximize structural efficiency. Small geometrical elements (fillets of small radius, texturing of surfaces, details of mounting bolts) were eliminated to cut the price of computation without altering aerodynamic performance. Figure 1 shows the CAD model of the halo.

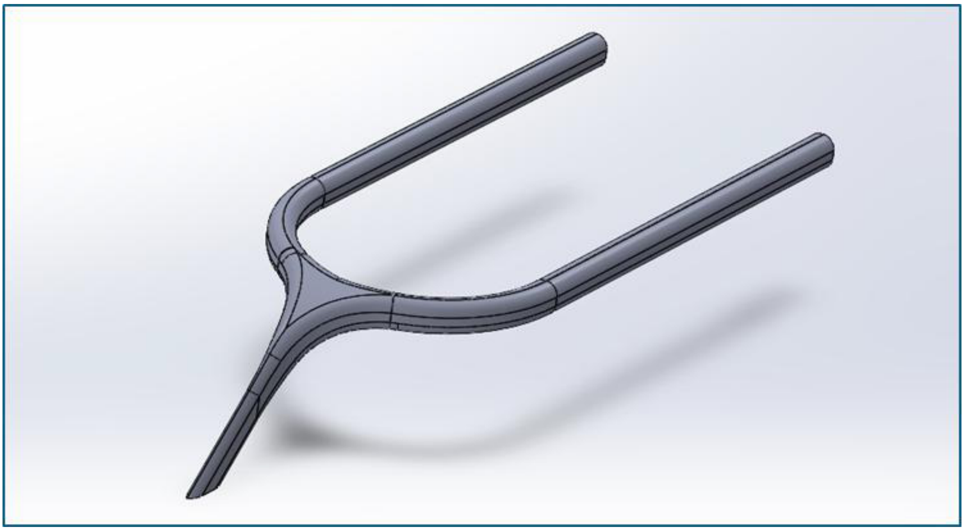

Fig. 1. CAD model of halo

2.2 Structural Analysis Framework

The ANSYS Workbench with implicit structural mechanics and 10-node tetrahedral elements with optimized mesh was used in the structural analysis. The mesh comprised about 50,000-100,000 elements having refined spacing around stress concentration areas and the pylon mounting point of the rear pylon was fixed at the boundaries. In the analysis, Young's modulus is 100MPa, Poisson's ratio 0.34, density 4430 kg/m3, yield strength 1030 MPa and ultimate tensile strength of 1160 MPa are considered. Three distinct FIA-mandated load cases were evaluated as reported in Table 1. Figure 2 represents a meshed model. Element type is 10-node tetrahedral and the total number of elements is 726,717.

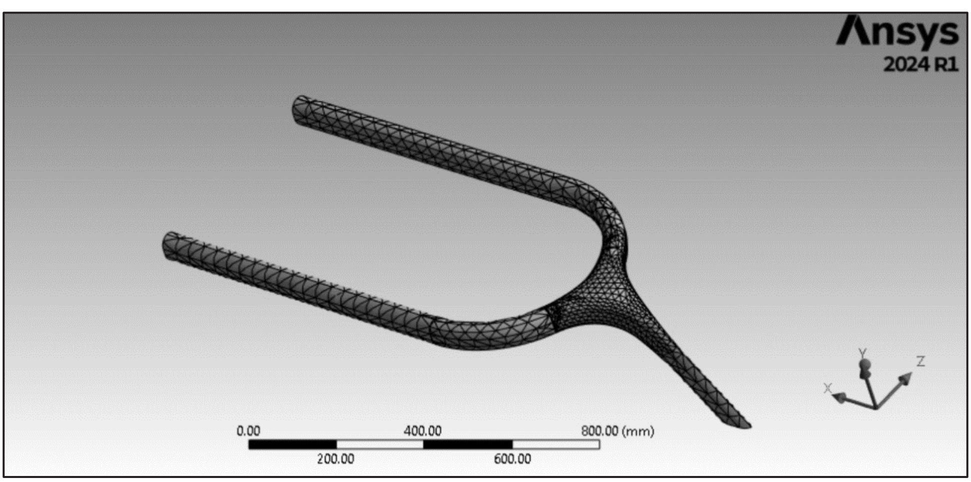

Fig. 2. Meshing of halo

Table 1. FIA-mandated load cases

Load Case	Applied Force	Location	Regulatory Limit
Vertical Static	125 kN	Forward arm (vertical direction)	$\delta \leq 3.0$ mm
Frontal	16 kN	Central Y-junction	$\delta \leq 3.0$ mm
Side	12.5 kN	Inner curve of the forward arm	$\delta \leq 3.0$ mm

2.3 Aerodynamic Analysis Framework

The Halo model was encircled in a rectangular computational area whose upstream length is five times the halo length to develop a complete inlet condition and downstream length is 10 × halo length so as to develop a full wake. The 5 times halo width was kept in both directions at the lateral extent. The hybrid method was a trade-off between accuracy and computational efficiency that used tetrahedral elements with the maximum edge length of 50 mm in the bulk domain and 5 inflation layers, optimizing y + to less than 1. Wake refinement decreased the size of elements by half of the bulk domain size, which gave around 726, 717 elements in total. Solver Configuration employed a pressure-based, steady-state approach with SST k-w turbulence model with low-Reynolds number corrections. Pressure-velocity coupling used a simple algorithm with second-order upwind discretization. Convergence criteria: Residuals < 10-4 for continuity and momentum; force monitor stability < 0.1% over 100 iterations. Reynolds number calculations at 30 m/s yielded Re = 1.85 × 105 (transitional to turbulent) and at 80 m/s yielded Re = 4.93 × 105 (fully turbulent). Both velocities operate in the fully turbulent regime, justifying the SST k-w model selection. Figures 3 and 4 depict the enclosure meshing and the meshing of the inflation layer.

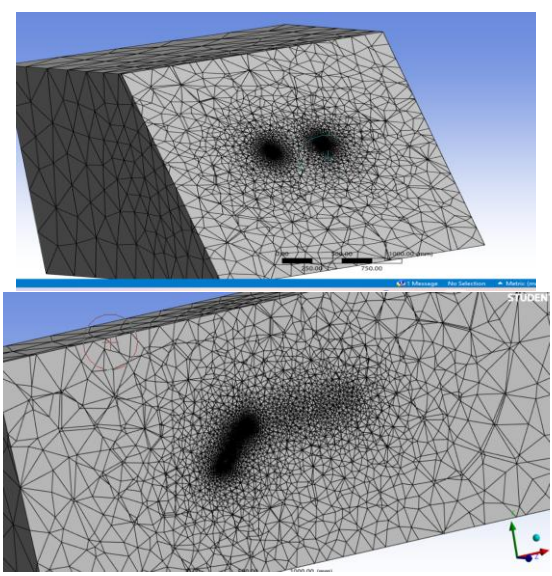

Fig. 3. Enclosure meshing (selection plane)

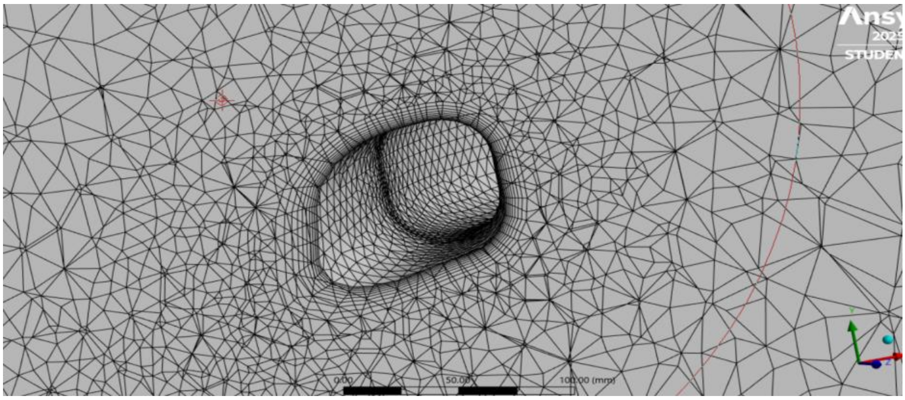

Fig. 4. Inflation layers (for better boundary layer visualization)

2.4 Modal Analysis Framework

Figure 5 represents the meshing of the halo. Modal analysis establishes natural frequencies and mode shapes by extracting eigenvalues by the use of fixed boundary conditions at the rear pylon mounting points. Six modes are Eigenfaced (enough to capture major vibrational properties), having a frequency range of DC to about 400 Hz.

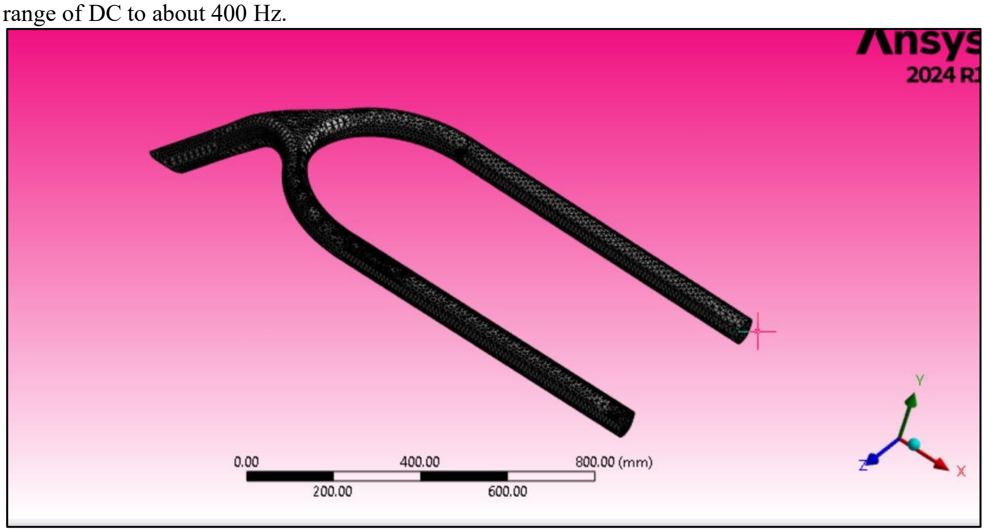

Fig. 5. Meshing of halo

3 Results and Discussion

3.1 Structural Analysis Results

The analysis is performed for a vertical static load of 125 kN. It exhibits the stress distribution concentrated on the area near the fixed support and an exponential distribution on the structure. A cantilever-like load condition gives rise to the cantilever-like stress state with maximum stress bending on the reaction. The deflection of 2.687 mm is 89.6 percent of the allowable deflection, which means that there is excellent stress distribution and sufficient rigidity. Table 2 represents the output for vertical load.

Table 2. Vertical static load result

Parameter	Value	Status
Maximum von-Mises Stress	399.14 MPa	Below yield (1030 MPa)
Maximum Deformation	2.687 mm	Below limit (3.0 mm)
Safety Factor	2.58	Above 1.0 requirement
Stress Location	Near fixed support (expected)	—

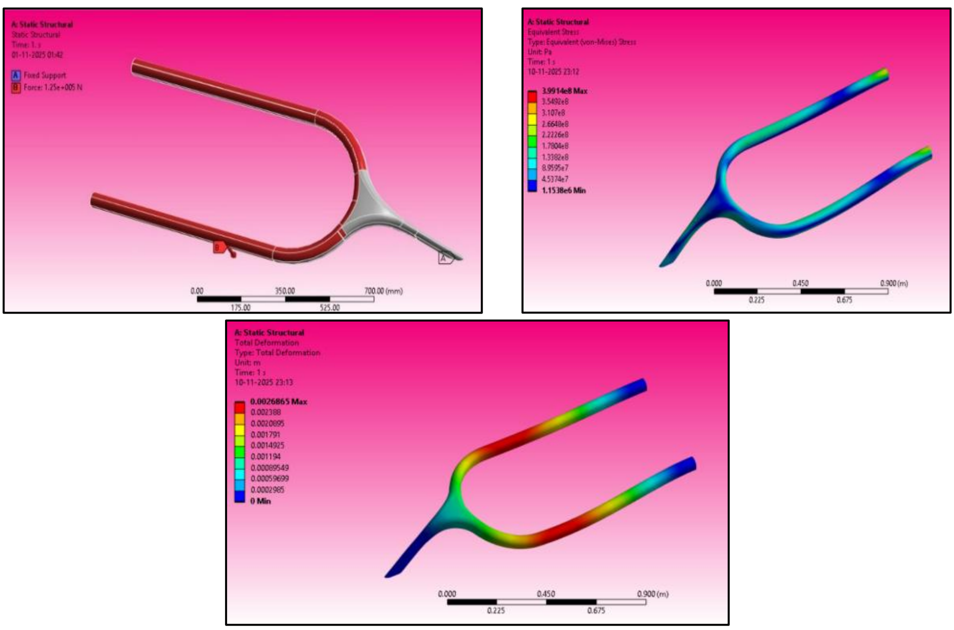

Fig. 6. Vertical static load result

Analysis is carried out for a 16 kN load applied at the frontal Y junction. Frontal load case results in minimum stresses compared to all the load cases. The largest concentration of stress appears at the place of loading (central Y-junction), where it quickly spreads to the connecting arms. The incredibly large safety factor (24.88) indicates that the load case is heavily over-designed as well, hence there is some potential to optimize this load case.

Table 3. Frontal load result

Parameter	Value	Status
Maximum von-Mises Stress	41.39 MPa	Below yield (1030 MPa)
Maximum Deformation	0.3554 mm	Below limit (3.0 mm)

Safety Factor	24.88	Substantial margin
Deformation Ratio	11.8% of allowable	—

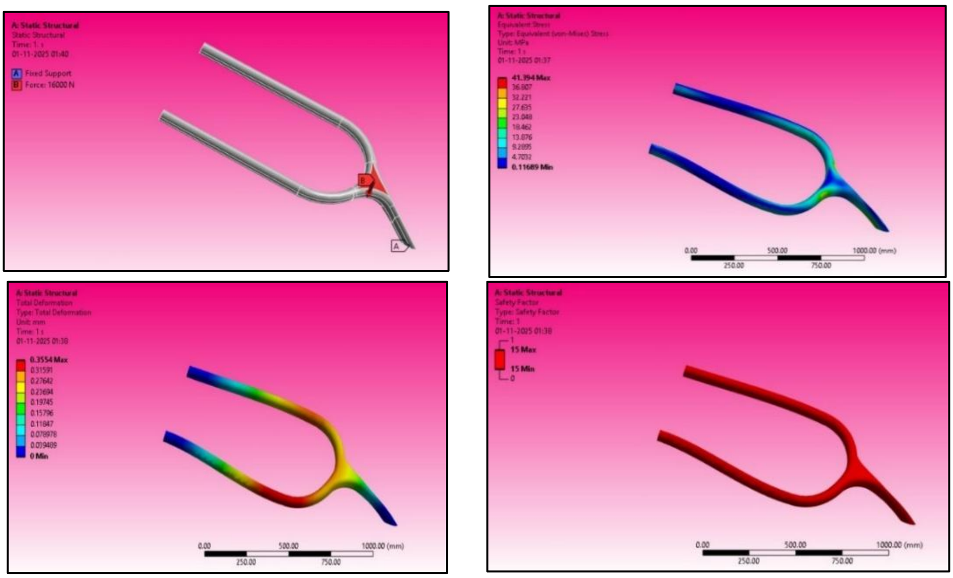

Fig. 7. Frontal load result

In the third case, a side load of 12.5 kN on the forward arm. It is seen that side loading has the greatest deformation ratio and a middle level of stress. Concentration of stress takes place at the rear fixed support, where the chassis is transferred to the rear. The deformation image substantiates anticipated cantilever-like actions, with the highest movement at the point of introducing the load.

Table 4. Side load result

Parameter	Value	Status
Maximum von-Mises Stress	121.68 MPa	✓ Below yield (1030 MPa)
Maximum Deformation	2.241 mm	✓ Below limit (3.0 mm)
Safety Factor	8.46	✓ Above requirement
Deformation Ratio	74.7% of allowable	—

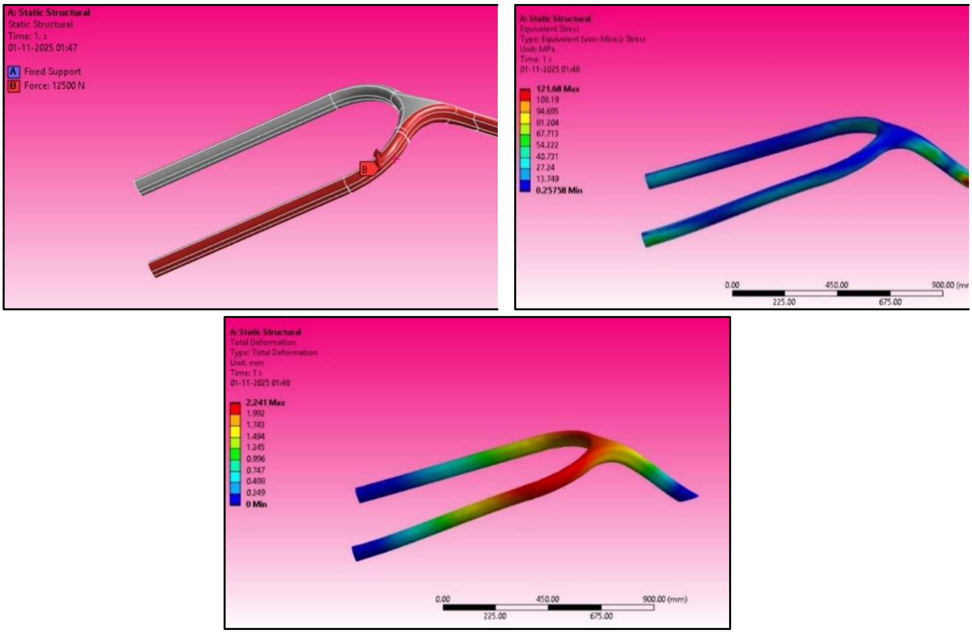

Fig. 8. Side load result

3.2 Aerodynamic Analysis Results

3.2.1 Force Measurements and Coefficients

The drag coefficient increases non-linearly with Reynolds number, from 0.368 at 30 m/s to 0.841 at 80 m/s. The velocity-squared scaling of dynamic pressure predicts a force ratio of 7.11, but the observed ratio of 16.25 indicates significant Reynolds number dependency.

$$R_e = \frac{\rho V L}{\mu} \quad (1)$$

The drag coefficient, in its non-linear relationship with Reynolds number, has a value of 0.368 at 30 m/s and 0.841 at 80 m/s. The scalability criteria of the dynamic pressure (velocity-squared) predict a ratio of 7.11 between the forces, but a ratio of 16.25 was found to show that the data is very significant.

Table 5. Aerodynamic coefficients at representative velocities

Velocity	Drag Force (N)	Lift Force (N)	Cd	Cl	Note
30 m/s	5.068	1.454	0.368	0.106	Low Re, separated flow
80 m/s	82.38	-12.53	0.841	-0.128	High Re, modified separation

3.2.2 Pressure Distribution Analysis

The front central pillar (impingement area where the velocity of flow is nearly zero) is a high-pressure area, as well as the forward-facing surfaces of the side arms. The low-pressure areas are determined on the backside of all structural members, the wake area behind the Halo, and flow separation areas and recirculation areas. At the representative racing speed (80 m/s), Halo's drag force is 82.38 N with the approximate total vehicle drag of 4000-5000 N, which contributes to its drag of 1.6-2.1%. This minor aerodynamic price can be easily accommodated by the vehicle-level aerodynamic optimization, and warrants the benefits that the protective structure offers in terms of safety.

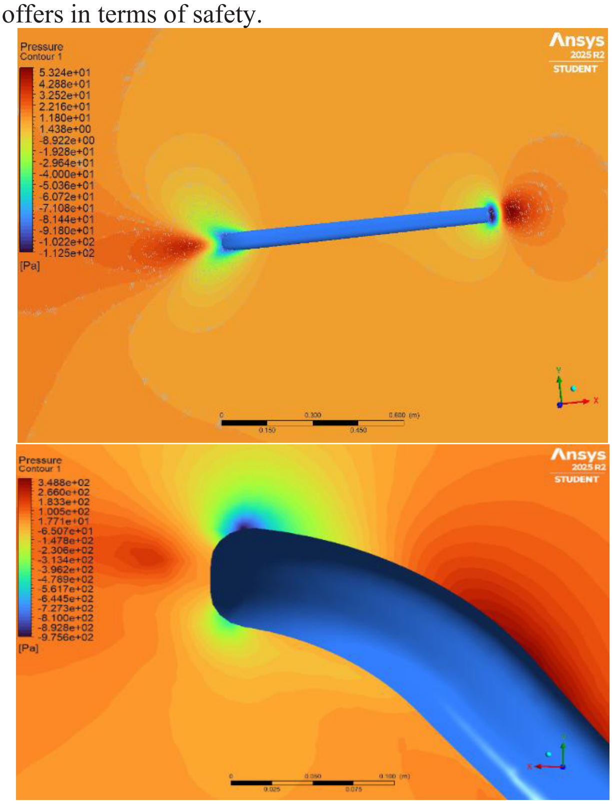

Fig. 9. Pressure contour for side tubes and front tubes

3.2.3 Pressure Distribution Analysis

The development of the boundary layers around the halo tubes is shown in Fig. 10. The mesh using the inflation technique was able to achieve the near-wall velocity gradients, with the thickness of the boundary layer rising in the direction of flow. The changed attitude of the attached to separated flow is very evident in the back parts of the halo arms. This boundary layer, which is effectively obtained using the CORE inflation mesh at a y+ of below 1, indicates that laminar secondary flow is exhibiting a turbulent nature, and separation is also taking place on the back surfaces as anticipated by the adverse pressure gradients.

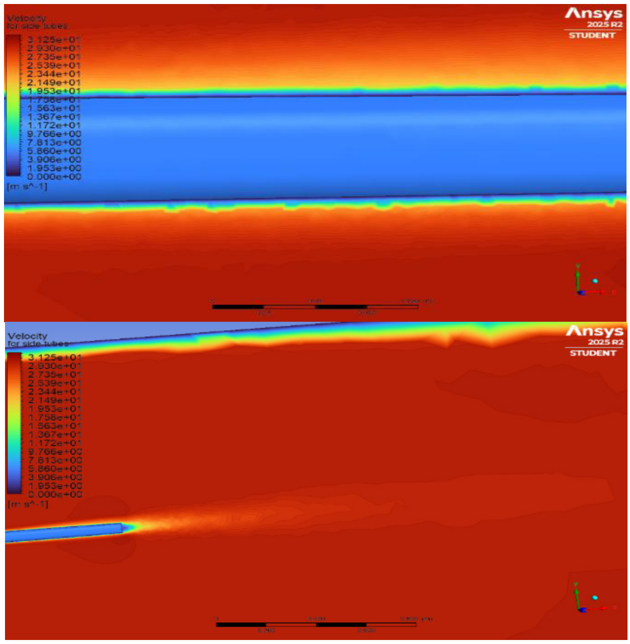

Fig. 10. Boundary Layer and Wake Region

3.2.4 Velocity Streamline Analysis

In Figure 11, velocity streamlines are displayed in colors of velocity magnitude. The streamlines provide some significant flow details. We are able to note flow separation between the core pillar and peripheral arms and acceleration between the shaped upper surfaces. On the rear surfaces, there is separation and recirculation and creation of wakes, including the shedding of vortexes (in reality, but steady-state simulation demonstrated a pattern that tended to time averaging). It is also observed to reattach flow several diameters lower.

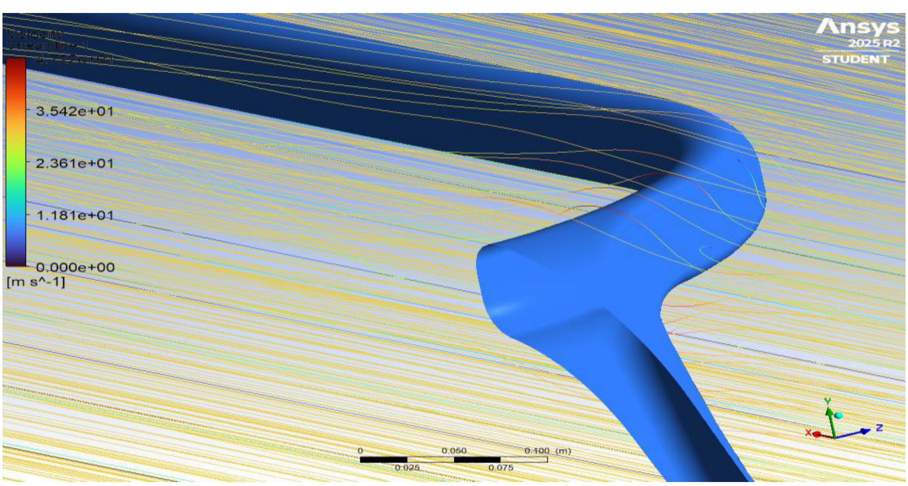

Fig. 11. Velocity streamlines

Besides the concept of a component being strong, the vibrational nature of a component also plays a vital role in a high-performance scenario such as Formula 1. The natural frequencies and mode shapes of the F1 Halo were determined by a Modal Analysis. This study is necessary to make sure that the building is not prone to resonance. Resonance will arise when ambient vibrations occurring in the engine, drive train, or even the track surface coincide with one of the natural frequencies of the Halo, which may result in higher, uncontrolled deformations and terminal fatigue failure.
They were analysed using the meshed model (Figure 12) with a rigid support attached to the rear pylon to provide the effect of its hard attachment to the monocoque chassis. The first six natural frequencies were obtained. The mode shapes and natural frequencies of the first six mode shapes were identified. These are the most effortless modes of vibration of the structure when excited.

Table 6. Result of Modal Analysis

Mode Number	Natural Frequency (Hz)	Mode Shape Description
Mode 1	63.814 Hz	First lateral bending (uniform side-to-side) of the hoop.
Mode 2	134.71 Hz	First vertical (out-of-plane) "flapping" of the arms.
Mode 3	154.15 Hz	Asymmetric vertical bending (arms flap in opposite directions).
Mode 4	216.67 Hz	Second-order lateral bending (S-shape) of the arms.
Mode 5	264.7 Hz	Complex twisting (torsional) and out-of-plane bending.
Mode 6	373.9 Hz	High-frequency, complex S-shape twisting of the arms.

The modal analysis was capable of determining the focus vibrational modes of the Halo. The natural frequency has its lowest point (63.814 Hz), which is much higher than the usual low-frequency vibrations caused by the track or tire imbalance (usually in the 5-20 Hz range), reducing the possibility of resonance by them. The following frequencies are properly distributed. The major issue with F1 is that the vibrations of the engines are experienced, and at the redline of 15000 RPM, the fundamental frequency becomes 250 Hz. It can be seen that the Mode 5 (264.7 Hz) of the Halo is near this primary engine frequency. Although the proximity may be an issue, there is a distinct distance between the other five modes. This suggests that the overall design is quite strong, although the connection between Mode 5 and the working frequency of the engine could be researched or damped more in a practical environment. Generally, the design shows that there is a low probability of catastrophic resonant failure.

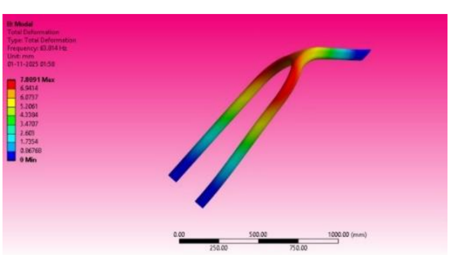

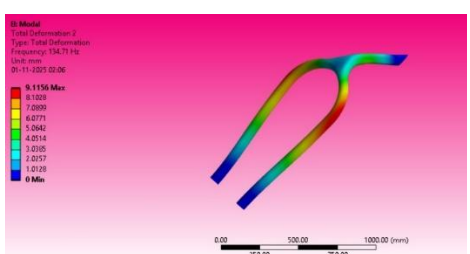

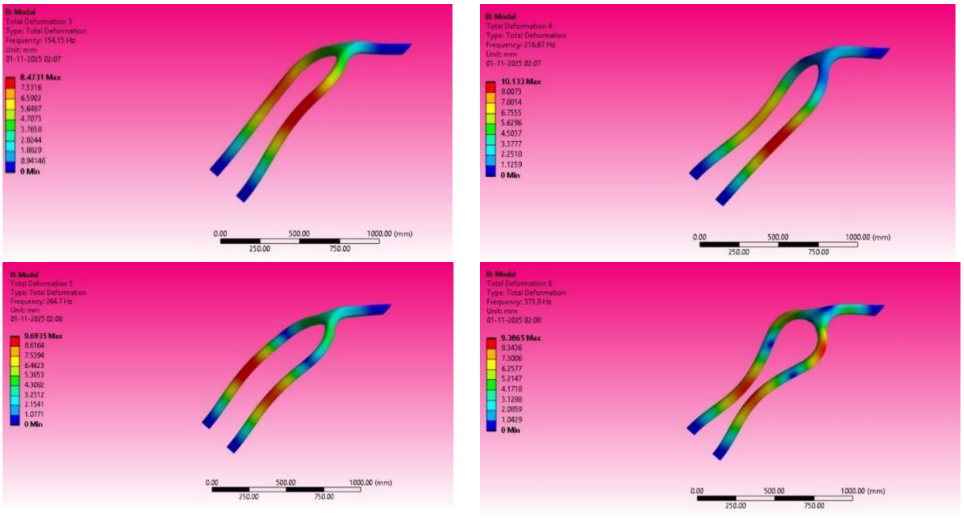

Fig. 12. Modal analysis

There are limitations of the current study. This computational study operates within specific constraints that merit acknowledgment. The steady-state hypothesis rules out effects of time-sensitive vortex shedding and transient aerodynamic effects. Isolated component analysis removes aerodynamic interactions at the vehicle level as well as the modification of the flow field by the vehicle; this is not everywhere considered part of full car geometry. The linear elastic analysis presumes that the material response is totally within the elastic regime, and there is no nonlinear response and no situation of plastic deformation. Moreover, modal analysis only records the linear behavior, with nonlinear effects such as large-deformation effects and material nonlinearity that are not taken into consideration. This work used simplified boundary conditions at the Halochassis interface with fully fixed support instead of flexible mounting systems, which could occur in engineering designs, and material properties were homogeneous titanium everywhere except for the manufacturing variation and the possible distribution of defects. Aerodynamic analysis conducted at constant velocity profiles does not account for yaw angle effects, crosswind conditions, or transient flow patterns encountered during cornering maneuvers. Structural analysis employed quasi-static loading without consideration of cyclic fatigue, impact dynamics, or combined multi-axis loading scenarios that occur during actual racing operations.

4 Results and Discussion

This computational study is fully integrated to provide validations of the Formula 1 Halo in structural, aerodynamic, and dynamic disciplines. Key findings include:

- Structural Robustness: With all FIA-authorized load cases, the Halo performs exceptionally in structural performance with peak stress (399.14 MPa) at 38.8 percent of the yield strength and the peak deformation (2.687mm) at 89.6 percent of the regulation limit. The safety factors lie between 2.58 and 24.88, which ensures there are significant design margins.
- Aerodynamic Feasibility: At 30 m, the Halo generates drag forces of 5.07 N and 82.38 N, which is 1.6-2.1 percent of total vehicle drag. Aerodynamic penalty is quite acceptable in the context of having a critical component in a safety feature and some opportunities to streamline it in the future were detected.

- Dynamic Stability: Modal analysis establishes natural frequencies between 63.814 Hz and 373.9 Hz and is effectively separated by the normal operation vibrations. The lowest natural frequency offers a wide margin over typical sources of disturbance, alleviating risk to resonance.
- Material Performance: Grade 5 Titanium (Ti-6Al-4V) is highly satisfactory since it has good strength-to-weight ratios, impact resistance and is compatible in manufacturing.
- Multi-Disciplinary Integration: The main structural, aerodynamic and dynamic studies set a complete framework of validation, evidencing effective integration of safety engineering and performance considerations.

References

1. FIA Technical Regulations, *Formula One Technical Regulations 2018* (Fédération Internationale de l'Automobile, Geneva, 2018)
2. S. Srinivasan, H.O. Demirel, Quantifying vision obstruction of Formula One (F1) halo concept variants, in *Proceedings of the 7th International Digital Human Modeling Symposium*, University of Iowa 7(1) (2022)
3. S.M. Rosalie, J.M. Malone, Women in motorsport: A case report of driving posture and performance after double mastectomy. *Phys. Ther. Sport* 36, 1–4 (2019)
4. H.O. Demirel, S. Srinivasan, A proactive ergonomics framework to assess A-pillar vision obstruction. *Digit. Hum. Model. Appl. Health Saf. Ergon. Risk Manag.* 46, 16 (2022)
5. M. Lin, P. Papadopoulos, Effect of halo protection device on the aerodynamic performance of formula racecar. *Int. J. Mech. Mechatron. Eng.* 14(1), 13–18 (2014)
6. A. Dhumal, N. Ambhore, P. Tamkhade, A. Marne, N. Mujawar, Numerical optimization for aerodynamic performance of nose cone of FSAE vehicle through CFD. *CFD Lett.* 16, 161–171 (2024)
7. M.M. Ghisheer, I. Esen, H. Ahlatci, B. Akın, Investigation of microstructure, mechanics, and corrosion properties of Ti6Al4V alloy in different solutions. *Coatings* 14(3), 277 (2024)
8. A. Szafrańska, A. Antolak-Dudka, P. Baranowski, P. Bogusz, D. Zasada, J. Małachowski, T. Czujko, Identification of mechanical properties for titanium alloy Ti-6Al-4V produced using LENS technology. *Materials* 12(6), 886 (2019)
9. M.A. Kumbhalkar, T.S. Sargar, S.H. Sarje, M. Sakhlecha, S. Prayagi, G. Gondhlekar, N.B. Kardekar, M. Sorte, Finite element analysis of paddler sludge dryer for its structural integrity under different loading conditions. *Int. J. Basic Appl. Sci.* 14(SI-2), 26–40 (2025). https://doi.org/10.14419/ddg57682
10. U. Ravelli, *Aerodynamics of a 2017 Formula 1 car: Numerical analysis of a baseline vehicle and design improvements in freestream and wake flows*, Master Thesis, Università degli Studi di Bergamo, Italy (2019)
11. K. Rangarajan, G. Velayudhan, Enhancing aerodynamic performance of a formula car through modification and evaluation, in *Proceedings of the International Conference on Trends in Automotive Parts Systems and Applications* (2024), 354537